

Ji Min Kim

Division of Advanced Nuclear Engineering,
POSTECH,
San 31, Hyoja-dong, Nam-gu,
Pohang 37673, Kyungbuk, South Korea
e-mail: erskarin@postech.ac.kr

Ji Hoon Kim

Department of Mechanical Engineering,
Incheon National University,
Songdo 1(il)-dong, Yeonsu-gu,
Incheon 22012, South Korea
e-mail: Kimjihoon123@inu.ac.kr

Moo Hwan Kim

Division of Advanced Nuclear Engineering,
POSTECH,
San 31, Hyoja-dong, Nam-gu,
Pohang 37673, Kyungbuk, South Korea
e-mail: mhkim@postech.ac.kr

Massoud Kaviany

Department of Mechanical Engineering,
University of Michigan,
Ann Arbor, MI 48109
e-mail: kaviany@umich.edu

Ho Seon Ahn¹

Department of Mechanical Engineering,
Incheon National University,
Songdo 1(il)-dong, Yeonsu-gu,
Incheon 22012, South Korea
e-mail: hsahn@inu.ac.kr

Nanocapillarity in Graphene Oxide Laminate and Its Effect on Critical Heat Flux

The nanocapillarity phenomenon involves ultralow frictional flow of water molecules through nanoscale channels, and here we study this using exceptionally large number of nanochannels within graphene oxide (GO) laminates. The nanoconfined water molecules in GO nanochannels form square lattice (as in the ice bilayer), which melts and jumps across the channels, similar to slip flow, with mean speed of the order of 1 m/s. This ease of liquid spreading in GO laminate is used to delay the critical heat flux (CHF) phenomenon in water pool boiling, by preventing formation/growth of dry spots. The water nanocapillarity speed is derived based on the measured water penetration flux, and the CHF enhancement (up to 140%) is demonstrated on a 1- μm -thick GO laminate. The GO laminate offers efficient surface modifications for increased transport efficiency (and safety margin) of pool boiling heat transfer systems. [DOI: 10.1115/1.4036282]

1 Introduction

Nucleate boiling, in which a vigorous phase change of liquid to vapor occurs on a hot, solid surface, is one of the most efficient heat transfer modes; heat flux of $\sim 1 \text{ MW/m}^2$ order can be transferred at a relatively low wall superheat temperature ($\sim 50 \text{ K}$). The CHF is the operating limit of the nucleate boiling regime, above which vapor acts as a thermal insulating layer, covering the entire heat transfer surface and preventing liquid phase change. It leads to a rapid temperature increase in the heating material, resulting in system failure; thus, CHF is a key parameter in determining the efficiency and safety of the system.

For this reason, additional water supply to prevent dry out region on the heating surface has been studied as an efficient strategy to delay the CHF phenomenon. A micro/nanostructured surface provides a dramatic enhancement of the CHF; this surface type has been analyzed in numerous studies in terms of the liquid supply and the enhancement of surface wettability. Methods for its preparation involve the fouling of nanoparticles for a porous layer [1,2], microelectromechanical system (MEMS) fabrication on a silicon wafer [3,4], and anodic oxidation of a metal plate [5]. Especially with a nanostructured surface showing a super hydrophilic surface with liquid-spreading phenomena, additional liquid can be supplied by means of capillary action to cool the heating surface so that dry out, triggering CHF, can be prevented [1,2,5,6]. By measuring the absorbed volume of liquid on the engineered surfaces, the CHF enhancement ratio or gain can be predicted successfully on the basis of Zuber's CHF model [7]. Accordingly, these

wetting features of surfaces have been discussed as key parameters in delaying CHF.

A graphene-coated surface has been reported as an efficient method for CHF enhancement [8–11]. When GO and reduced GO colloidal suspensions were used as working fluids in the nucleate boiling, the graphene flakes were self-assembled along the liquid–vapor interface of bubbles. The arranged GO and reduced graphene oxide (RGO) flakes close to the heating surface were deposited on it, resulting in two-dimensional (2D) [12,13] and three-dimensional (3D) [10] graphene structures, respectively; the CHF was enhanced dramatically. However, these graphene-coated surfaces showed mostly poor wettability. This indicated that the wettability analysis for CHF enhancement discussed above could not solely explain the CHF enhancement on graphene-coated surfaces. As such, other explanations have also been investigated, including Rayleigh–Taylor (RT) instability [8,9], liquid-saturated porous media [10], and thermal activity [11–13].

In our previous study [12,13], pool boiling performance of GO colloidal suspension was reported; GO flakes formed a 2D laminate structure with well-aligned flakes, and its thickness had a close relationship with the CHF enhancement ratio. The GO laminate was postulated as a heat spreader to disperse locally overheated region, i.e., hot spot, whereby a modified CHF correlation was derived, based on the thermal activity analysis [13,14], as shown in Table 1. In this study, a new approach was tried; the GO laminate was postulated as a liquid supply channel whereby liquid inflow rate was derived into the CHF enhancement gain, based on energy balance, with sharing data of [12,13].

The GO laminate structure is an unimpeded membrane for water, with ultrafast water transport [17]. In a GO laminate film prepared by unidirectional flow deposition in vacuum filtration, water molecules and small ions ($< 4.5 \text{ \AA}$) are only able to penetrate the nanochannels between GO flakes, with a few thousand

¹Corresponding author.

Manuscript received August 19, 2016; final manuscript received March 9, 2017; published online April 25, 2017. Assoc. Editor: Ronggui Yang.

Table 1 Correlations of the CHF enhancement ratio or gain by analysis of absorbed volume of liquid on the engineered surfaces and graphene surface

Author/analysis	Correlation	Equation description
CHF correlation based on absorbed volume of liquid on the engineered surfaces Zuber [7]	$q''_{CHF} = K \cdot h_{lg} \rho_g^{0.5} [\sigma g (\rho_l - \rho_g)]^{1/4} + q''_{gain}$ $K = 0.131$	δ = thickness of graphene film δ_{porous} = thickness of porous layer ε = porosity
Kim and Kim [1]	$K = \left(\frac{1 + \cos \theta_r}{16} \right) \left[\frac{2}{\pi} + \frac{\pi}{4} (1 + \cos \theta_r) \cos \phi \right]^{1/2}$ in Ref. [15] $q''_{gain} = \frac{h_{lg} \rho_l}{4r_b^2} \varepsilon (2\pi r_b \sin \theta^* \delta_{porous}) u, u = \sqrt{L_c g}$	θ_r = receding contact angle θ^* = apparent contact angle
Rahman et al. [2]	$K = C \times \frac{\dot{V}''_{0\rho l}}{\rho_g^{0.5} [\sigma g (\rho_l - \rho_g)]^{1/4}}$	λ_m = modulated instability
Ahn et al. [5]	$K = C \times \left(\frac{1 + \cos \theta_r}{16} \right) \left[\frac{2}{\pi} + \frac{\pi}{4} (1 + \cos \theta_r) \cos \phi \right]^{1/2}$ in Ref. [15] $q''_{gain} = \frac{1}{4} \pi (0.8 R_{curv})^2 \bar{\theta}_r^3 \left(3 \bar{\theta}_r \frac{dR_{curv}}{dt} + 4 \cdot 0.8 R_{curv} \frac{d\bar{\theta}_r}{dt} \right) \rho_l h_{lg} / A_h$	ϕ = inclined angle of heater surface ρ = density σ = surface tension c = specific heat capacity
CHF correlation on graphene surface		C = fitting factor h_{lg} = latent heat k = thermal conductivity L_c = capillary height r_b = radius of bubble R_{curv} = curvature of droplet being absorbed into surface
RT instability [8,9,16]	$K = \frac{3[\sigma/g(\rho_l - \rho_g)]^{1/4}}{\lambda_m^{1/2}}$	u = velocity of liquid inflow
Thermal activity [11–14]	$K = 1.5026 \frac{S}{S + 0.007} + 1, S = \delta \sqrt{\rho_l c_h k_h}$	\dot{V}'' = absorbed liquid volume rate

times the transport speed versus the bulk diffusion speed [18,19]. This unique characteristic assumes that the water molecules in the nanochannels have a nearly frictionless flow, in which the water molecules are confined by the nanochannels so that they are dominantly affected by the van der Waals force as the driving capillary force [17,20]. Caupin et al. [21] reported that even though a material may show apparent hydrophobic wetting characteristics, like pristine graphene, it is possible to have a strong capillary force, depending on the geometry where the water molecules are confined. For example, a one-dimensional (1D) carbon nanotube and a 2D graphene nanochannel were expected to have 191 and 99.3 km of capillary height of water, respectively, based on the molecular potential energy analysis. This phenomenon is known as nanocapillary action. Simulations with molecular dynamics (MD) show that the equivalent capillary pressure and water penetration speed were ~1000 bar and ~10 m/s, respectively [17,18,22–24]. For this reason, GO films have attracted interest for use as membranes for molecular sieves with a water solvent [18,25–27]. Accordingly, as a new explanation, we propose that a GO laminate could act as a water supply channel to a dried out region via nanocapillarity to prevent CHF.

The objective of this study was to estimate the nanocapillary speed of water molecules experimentally via the nanochannels of a GO laminate, and consequently, predict CHF enhancement according to the thickness of the GO laminate film. Thus, a GO laminate film is proposed as a coating material for heating surfaces with liquid water supply in a nucleate boiling heat transfer system, as a new application.

2 Experimental

2.1 Preparation of GO Colloids. GO colloids were prepared via chemical exfoliation, based on a modified Hummer method [28], using the chemical oxidation of graphite and sonication procedures. Briefly, graphite powder (2 g), sodium nitrate (1 g), and potassium permanganate (6 g) were mixed at 35 °C for 2 h. Then,

distilled water (de-ionized (DI), 100 mL) was added and allowed to heat up to 98 °C, resulting in a yellow–brown mixture. The mixture was diluted with additional DI water (300 mL) and hydrogen peroxide (3%, 40 mL), washed three times with vacuum filtration, and then freeze-dried to a powder form. The GO powder was exfoliated in DI water by ultrasonication for 1 h, resulting in 0.5 mg/mL of GO solution (see Sec. S1, which is available under the “Supplemental Materials” tab for this paper on the ASME Digital Collection, for details).

GO colloids used in boiling experiments showed a transparent brown color (Fig. 1(a)). For transmission electron microscopy (TEM) analyses, GO flakes were sieved with a holey carbon grid. Figure 1(b) shows that the GO flakes had a 2D form, similar to a

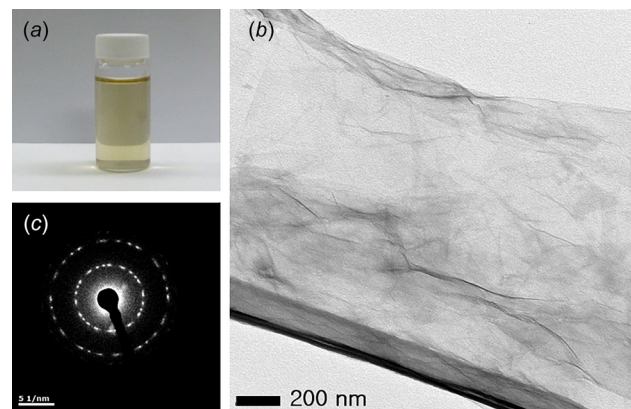


Fig. 1 (a) Graphene oxide (GO) colloids showed a transparent brown color, (b) GO flakes showed a two-dimensional (2D) monolayer structure in transmission electron microscopy (TEM) images, where the hexagonal sp^2 bonding structure of carbon atoms was damaged in the chemical oxidation process, as seen in, and (c) the selected area electron diffraction (SAED) image

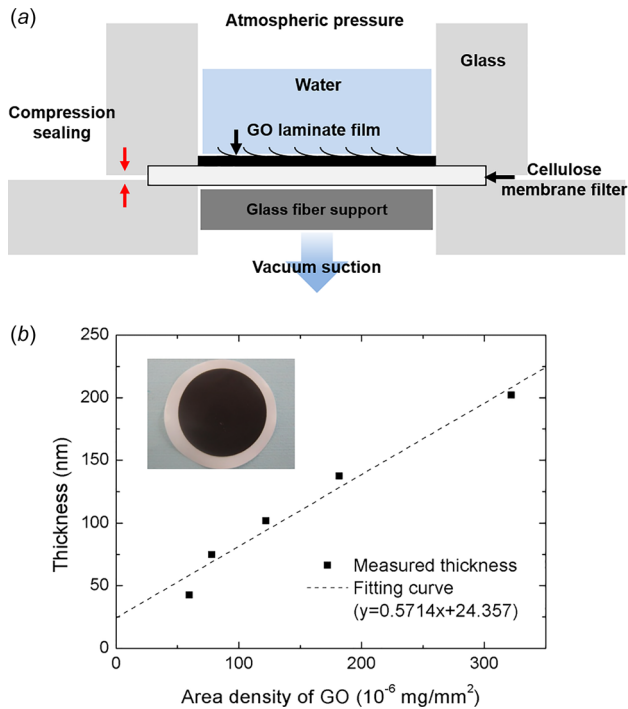


Fig. 2 (a) Schematic diagram of the water penetration experiment with vacuum suction and (b) thickness of GO laminate versus area density of GO (inset) an image of a GO laminate film on a membrane filter

sheet. Figure 1(c) shows an amorphous ring in a selected-area electron diffraction (SAED) image. This pattern was caused by the folding of sheets or defects in basal graphene surfaces, indicating that the hexagonal structure of carbon atoms with sp^2 bonding of GO flakes was damaged by chemical oxidation.

2.2 Water Penetration Experiment. Water penetration experiments were designed to measure the water flow rate via the GO laminate film (Fig. 2(a)). GO laminate films with uniform thickness were prepared by vacuum filtration of GO colloids using a cellulose membrane filter (Fig. 2(b)). The experimental apparatus consisted of three parts: (i) an upper glass container in which DI water (300 mL) was stored and its loss by penetration via the GO film was observed with a camera and gradations on the container; (ii) a membrane part in which the prepared GO laminate film was mounted, where the penetration phenomenon occurred; and (iii) a bottom glass container in which DI water suction was induced by a vacuum line (gauge pressure: -0.8 bar).

GO laminate films with a uniform thickness were prepared via unidirectional flow [29] for water penetration rate measurements. A cellulose membrane filter (Advantec, $0.45 \mu\text{m}$) was used for the preparation with vacuum suction. We varied the thickness of the GO film by controlling the amount of GO colloids at 0.5 mg/mL , dispersed in 100 mL of DI water for uniformity of film thickness by slowdown of deposition rate. The GO film thickness with respect to the amount of GO colloids was determined as follows:

$$\delta_{\text{film}} = \frac{V_{\text{colloids}} c_{\text{colloids}}}{\pi r_{\text{film}}^2 \rho_{\text{GO}}} \quad (1)$$

where δ_{film} is the GO film thickness, V_{colloids} is the volume of the GO colloids, c_{colloids} is the concentration of the GO colloids (0.5 mg/mL), r_{film} is the radius of the GO film (20 mm), and ρ_{GO} is the density of GO. Here, the density of GO was 1750 kg/m^3 , evaluated from trend line of Fig. 2(b) (surface profiler, Bruker DEKTAK XT-E), close to the value of 1800 kg/m^3 in the literature [29]. The inset of Fig. 2(b) shows a GO laminate film

prepared on a cellulose membrane filter; GO films of various thicknesses (62.5 , 126.2 , 252.4 , 757.1 , and 1388.1 nm) were prepared for measurements of the water penetration rate.

Next, 300 mL of DI water and a GO laminate film were prepared to set up the experiment. After the first 100 mL of DI water had passed through the GO film, the time for the next 100 mL of water to penetrate the GO film was measured for steady-state data, by taking images of the water level using gradations on the container (see Sec. S2, which is available under the “Supplemental Materials” tab for this paper on the ASME Digital Collection, for details).

2.3 Pool Boiling CHF Experiment. This paper shared CHF results on the GO laminate film from our previous study [13], so the experimental conditions were briefly summarized here. CHF experiments were conducted on a mirror-polished silicon wafer plate, $25 \text{ mm} \times 20 \text{ mm} \times 0.475 \text{ mm}$, with a 500-nm -thick silicon dioxide layer for electrical insulation, and a platinum film heater on the underside for Joule heating. The electrical resistance of the platinum film was calibrated with respect to the temperature (range: $100\text{--}150^\circ\text{C}$) for wall temperature measurements. The main plate heater was installed in a pool-boiling chamber, where 3.5 L of working fluid (DI water or GO colloids) could be saturated at atmospheric pressure after 2 h of preboiling (Fig. 3). The main heater was connected to a reference resistance and direct current (DC) power, whereby the voltage and current applied to the platinum film were measured to calculate the heat flux and wall temperature.

Experiments were carried out by increasing the applied heat flux to the main heater in steps after obtaining steady-state heat flux data and wall temperature data over a period of 2 min (see Fig. S3, which is available under the “Supplemental Materials” tab for this paper on the ASME Digital Collection); the data were space-averaged over the entire main heater for representative steady-state data. Thus, the boiling performance was characterized with space-time-averaged data. Accounting for the errors of the data acquisition system, the maximum uncertainties of the heat flux and wall temperature were determined to be less than 15 kW/m^2 and 1.5 K , respectively, for the expected CHF range (see Sec. S3, which is available under the “Supplemental Materials” tab for this paper on the ASME Digital Collection, for details).

To control the surface morphology modulated by GO deposition after nucleate boiling, various concentrations of GO colloids were used: 1 , 5 , and 10 mg/L ; the performance for each colloid concentration was compared with that of DI water as a reference case. Each case, including the DI water case, was repeated three times and averaged (see Sec. S4, which is available under the “Supplemental Materials” tab for this paper on the ASME Digital Collection, for details).

3 Results and Discussion

GO flakes were deposited on the surface by repeated nucleate bubbling, in which boiling characteristics could be enhanced, especially CHF performance. After GO boiling, a gray-colored thin film formed (Fig. 4(a); see also Sec. S5, which is available under the “Supplemental Materials” tab for this paper on the ASME Digital Collection). The atomic force microscopy (AFM) image in Fig. 4(b) shows that GO flakes $1 \mu\text{m}$ in length (inset) were deposited layer by layer. GO flakes have a negative charge in colloids due to the oxygen (i.e., carboxyl) groups, such that they repulse each other and finally form close-packed structures, such as laminates, when they are deposited by boiling [12,29,30]. Moreover, Figs. 4(c) and 4(d) show scanning electron microscopy (SEM) top-view and cross-sectional view images of a cracked GO film, respectively; overall, the $1\text{-}\mu\text{m}$ -thick GO film had a laminate structure.

Figure 5 shows pool boiling experimental results [13], where three experiments were conducted for each concentration. Here, every case was repeated three times and averaged, and the arrows indicate CHF points. The GO laminate film showed CHF

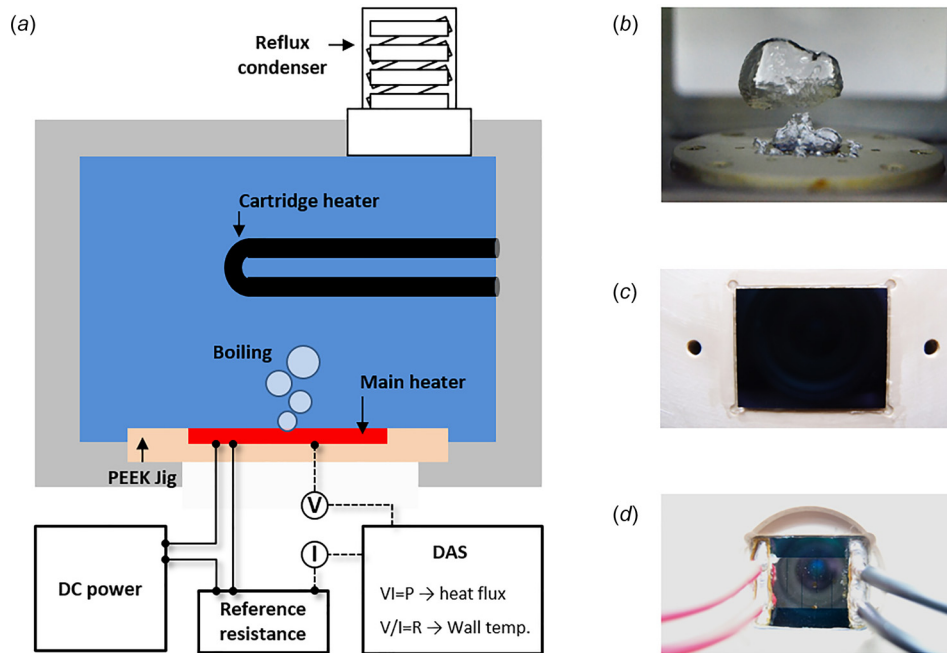


Fig. 3 (a) Pool-boiling experimental apparatus, (b) image of nucleate boiling on the main heater, (c) upper side, and (d) underside view of the main heater, showing the mirror-polished silicon plate with a platinum film heater on its underside

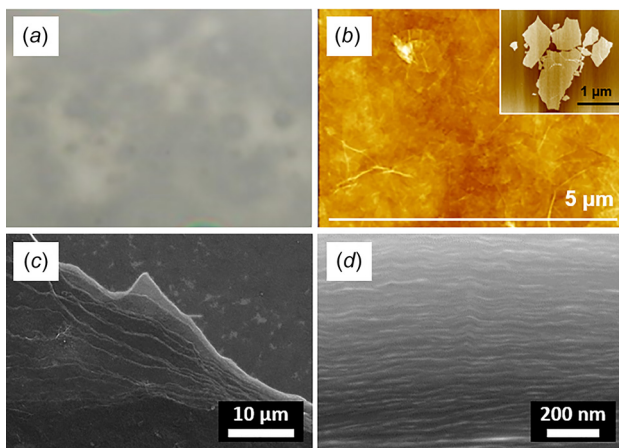


Fig. 4 Morphology of the GO laminate formed by boiling: (a) GO-coated surface (gray) after experiments, (b) atomic force microscopy (AFM) image of GO film and GO flakes (inset). Scanning electron microscopy (SEM) images of, (c) the top view of a region damaged by critical heat flux (CHF), and (d) its cross section, providing evidence that GO has a well-aligned laminate structure.

enhancement—by 94% (1 mg/L), 140% (5 mg/L), and 105% (10 mg/L)—versus pure water; clean silicon dioxide surface. The static and dynamic contact angles did not show significant differences with those on a bare silicon dioxide surface (see Fig. S6, which is available under the “Supplemental Materials” tab for this paper on the ASME Digital Collection); instead, Fig. 6 shows a close relationship between the CHF performance and the thickness of the GO laminate. The thickness was measured using SEM (Fig. 4(d)); specimens were prepared by additional boiling experiments for coating at 90% of the CHF because the CHF destroyed the GO laminate structures (see Sec. S7, which is available under the “Supplemental Materials” tab for this paper on the ASME Digital Collection). According to its thickness, the CHF performance increased rapidly initially and then slowed gradually,

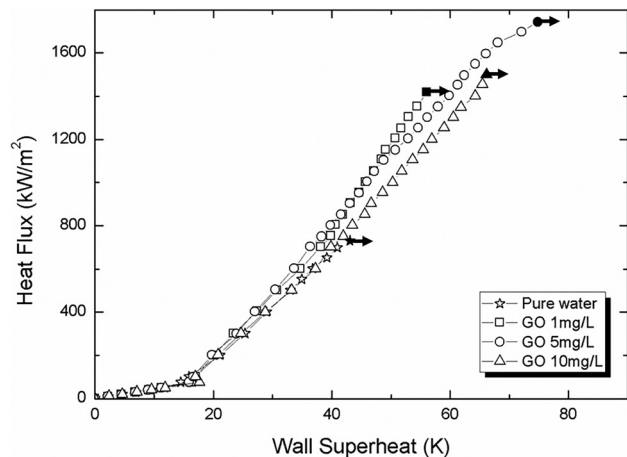


Fig. 5 Boiling curve; case of 1 mg/L, 5 mg/L, and 10 mg/L [13]

consistent with the CHF performance using a reduced GO (RGO) film [11]. Thus, we focused on the thickness of the GO laminate as a major parameter in CHF enhancement to investigate the effect of nanocapillarity via the GO laminate. Concentration was not directly related to the thickness of the GO laminate after boiling experiments: the 5 mg/L case showed a higher thickness than the 10 mg/L case. It was supposed that too rapid deposition of GO flakes could cause insufficient buildup of the laminate structure, as discussed in our previous report [13].

The CHF trigger is closely affected by the area of the vapor stem on the heating surface [31]. Compared with the bare surface in Fig. 7(a), a modulated surface with a GO laminate could manage the formation of a dry vapor region under a mushroom to prevent CHF triggering, even under higher heat flux conditions (1200 kW/m² versus 700 kW/m² bare) and a larger area of vapor coverage (Fig. 7(b)). Thus, we considered that liquid supply, by nanocapillarity through the GO laminate film under the mushroom in nucleate boiling, could prevent the formation of dry vapor regions, resulting in CHF enhancement (Figs. 7(c)–7(e)).

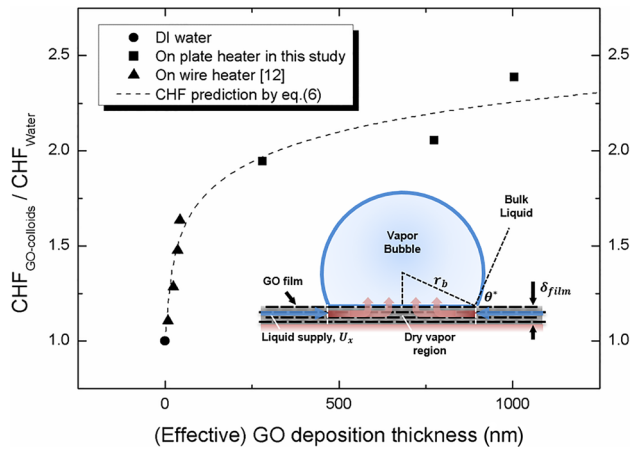


Fig. 6 CHF as a function of the thickness of the GO laminate and its prediction by nanocapillarity using Eq. (6). (Inset) schematic diagram of nanocapillary inflow into a dry-out zone during bubble growth on the GO laminate.

Our final goal in this study is to demonstrate an attainable heat flux gain by estimation of cross-sectional area and water-molecular penetration speed via effective nanochannel of the GO laminate beneath the mushroom. In order for that, we supposed a unit square cell with departing bubble diameter as its side length (Fig. 7(c)), then the heat flux gain could be estimated by water

penetration rate via perimeter of departing bubble (Fig. 7(d)). The inset in Fig. 6 shows a schematic diagram of the nanocapillary inflow via a GO laminate into a dry vapor region to prevent CHF triggering. The water penetration rate, Q , through the base of a departing bubble with radius r_b is as follows [1]:

$$Q = \varepsilon 2\pi r_b \sin \theta^* \int_0^{\delta_{\text{film}}} U_x dx \quad (2)$$

where ε is the porosity, θ^* is the receding contact angle, δ_{film} is the thickness of GO laminate, and U_x is the nanocapillary speed. Here, the second term is the perimeter and the third term is the water inflow rate via the entire GO laminate film, which should be integrated over the entire thickness of the GO laminate (the reason will be discussed later). Accordingly, following questions should be discussed for Eq. (2): (1) state and arrangement of water molecules confined in nanochannels between GO flakes to define the effective nanochannel for water penetration; (2) evaporation of water molecules on the GO laminate film near-CHF condition; (3) maximum speed of water molecules in the GO laminate with respect to thickness.

First, how water molecules could be arranged in nanochannels between GO flakes was discussed in order to define the effective nanochannel for water penetration. Boukhvalov et al. [23] described an ultrafast penetration phenomenon of water molecules into a GO laminate, with energy-based molecular dynamic (MD) simulations. They showed that only when nanoconfined water molecules in the GO nanochannels form ice bilayers, rather than

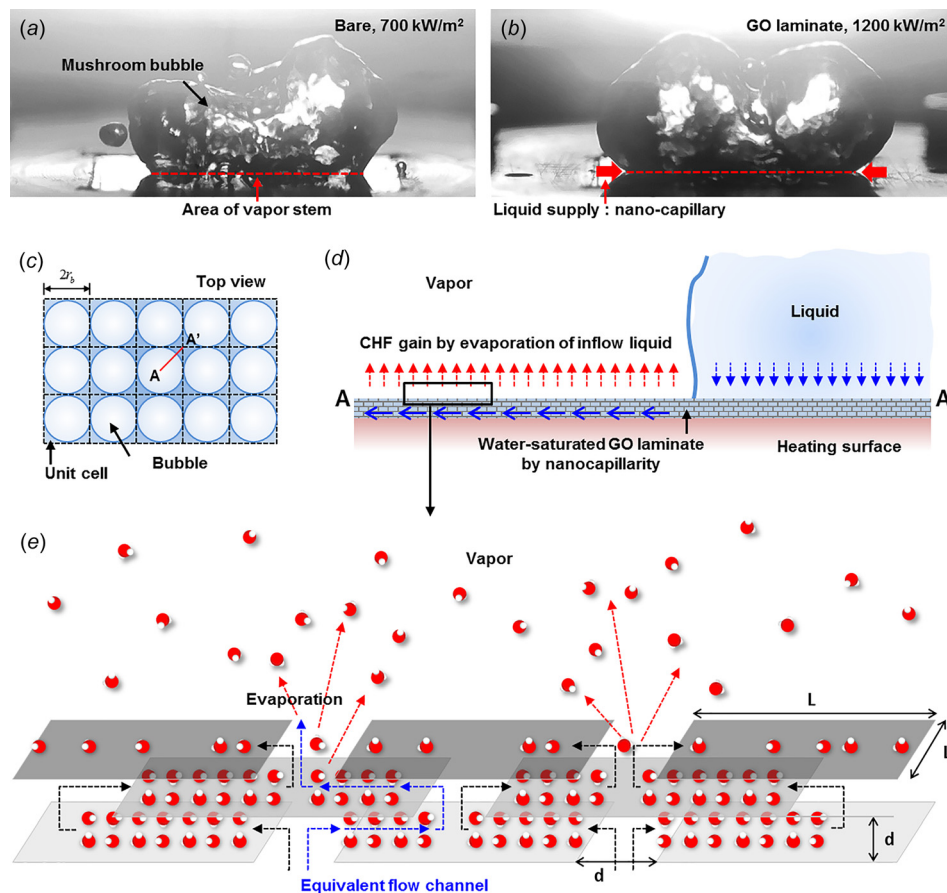


Fig. 7 Effect of a GO laminate film on CHF enhancement: high-speed visualization images of boiling under near-CHF conditions using de-ionized (DI) water on (a) a bare surface (700 kW/m^2) and (b) the prepared GO laminate (1200 kW/m^2), indicating that it could delay CHF, despite a higher area of vapor stems. Schematic diagram of nanocapillary inflow via the GO laminate underneath the mushroom, (c) top view, (d) side view in a unit cell, and (e) evaporation on top of the GO laminate. (See figure online for color.)

monolayer, they melt and jump into other channels at the edge of the flakes in which carboxyl groups had formed. This allowed fast water penetration across the GO laminate film to be realized. Then, the interlayer distance between GO flakes became important for the space occupied by water molecules, and it was predicted to 9 Å, which was believed to have a bilayer of water molecules [18,24]. The interlayer distance measured using X-ray diffraction (XRD) was 13 Å at a relative humidity (RH) of 100% to prepare water molecules-saturated GO laminate for optimal water penetration. This measurement was consistent with MD simulations, because the GO flakes themselves occupied ~ 4 Å of the thickness, with an optimal effective interlayer distance of 9 ± 1 Å [17,32,33].

Recently, Algara-Siller et al. [34] observed a nanocapillary phenomenon with mono-, bi-, and trilayers of water molecules between graphene films prepared using chemical vapor deposition, with transmission electron microscopy (TEM). The nanoconfined water molecules formed square ice, mostly with AA stacking, as opposed to the conventional tetrahedral structure with hydrogen bonding. The regular square lattice of water molecules maintained a continuum state, which was suggested to indicate that the interaction between water and graphene was weaker than that between water molecules.

The most important parameter in the nanocapillarity of water molecules is the interlayer distance [17,18,35]. It is worth to mention that GO can be reduced thermally under boiling circumstances, such that the interlayer distance between GO flakes becomes shorter. According to RH, water molecules could reversely get in and out of the GO nanochannels, resulting in the change of interlayer distance; the criteria of interlayer distance at RH = 0% were reported to be near 7 Å at RH = 0%. For GO laminate showing above the criteria, its interlayer distance increased to 13 Å at RH = 100% by intercalation of water molecules, such that nanocapillary flow would be possible [17,32,33]. So, it measured the interlayer distance of GO flakes in the GO laminate formed by nucleate boiling in order to confirm whether it could form a bilayer of water molecules. Figure 8 shows measured XRD patterns of GO laminates prepared by boiling and by vacuum filtration in a dry state (i.e., RH = 0%). The (002) peak of the boiling specimen was at $2\theta = 12.62$ deg, corresponding to an interlayer

distance of 7.011 Å; the vacuum filtration specimen showed the peak at $2\theta = 12.14$ deg, with an interlayer distance of 7.205 Å. These values indicated that the interlayer distance in the GO laminate with boiling had decreased slightly by thermal reduction, and X-ray photoelectron spectroscopy (XPS) analysis also showed a decrease in oxygen bonding in the GO laminate with boiling (see Fig. S9, which is available under the “Supplemental Materials” tab for this paper on the ASME Digital Collection). But the interlayer distance data showed that the GO laminate with boiling was able to form a bilayer of water molecules. It was consistent with the previous report [35], in which intercalation of water molecules could still occur reversibly onto GO flakes after mild thermal reduction at 100 °C

Given these findings, we sought to estimate the nanocapillary speed of water molecules under circumstances whereby (i) all of the nanochannels in the GO laminate were filled with a bilayer of water molecules and (ii) the nanoconfined water molecules passed through the channels by forming a square ice lattice (i.e., the blue arrow in Fig. 7(e)).

Second, evaporation of water molecules on the GO laminate film was discussed in order to define the critical condition of nanocapillarity near-CHF condition. Duan et al. [36] reported physics on evaporation of water in nanochannels with 20 nm to 105 nm of height. The evaporation rate in nanochannel was dominantly limited by vapor diffusion from liquid–vapor interface through the channel and was closed to a phase pattern consisting of liquid, vapor, and their interface, i.e., existence of cavity in liquid filled nanochannel. However, the evaporation on the GO laminate was postulated to occur only at the its top surface (Fig. 7(e)), because the necessary condition to open nanochannels in the GO laminate to deliver water molecules is sufficient saturation with water molecules. Therefore, the situation in which water molecules escape the nanochannel in the GO laminate by breaking the interaction with graphene surfaces at a certain critical condition (i.e., high temperature) is supposed as a breakdown of nanocapillarity for water. It means the GO laminate could not act as a liquid supplying channel, resulting in the CHF phenomenon. In these reasons, any cavitation in nanochannel in the GO laminate would not be considered in boiling phenomena before CHF.

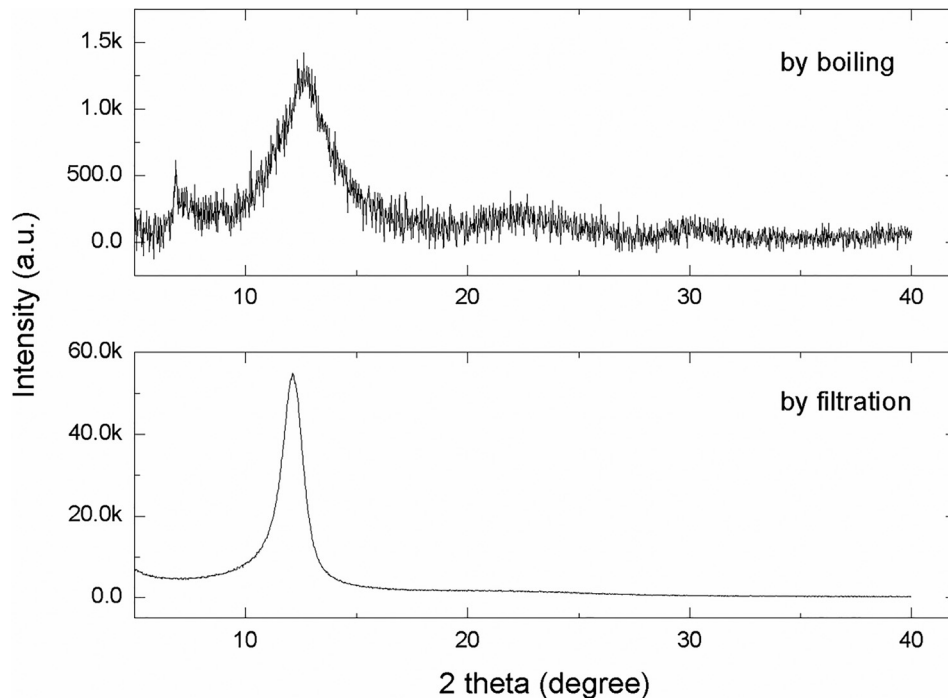


Fig. 8 Plot of the measured X-ray diffraction (XRD) pattern of the GO laminate by boiling and by filtration

Then, when a superheated water molecule exited from the open end of the nanochannel at the top surface of the GO laminate by evaporation, how fast the vacancy could be filled by neighboring water molecules with continuum ice lattice between GO flakes? In other words, how fast GO laminate could absorb water molecules to maintain its saturation for acting of liquid supply channel would be the third question; maximum speed of water molecules in the GO laminate with respect to thickness to evaluate the CHF gain by nanocapillarity. If the evaporation rate became larger than the inflow rate, the surplus heat would increase wall temperature. It could lead to deactivation of nanocapillarity, and breakdown of liquid supply channel of the GO laminate, because the oxygen amount on GO was reported to decrease rapidly above 160°C, resulting in the decrease in the interlayer distance between GO flakes [35]. The CHF caused a damage of the GO laminate; a blow off, which seemed to have a relationship with the released water molecules [13]. Therefore, the nanocapillary speed U_x was discussed according to the thickness of the GO laminate due to its close relationship with the CHF (Fig. 6).

To estimate the nanocapillary speed of the water molecules, water penetration rates were measured as a function of the GO laminate thickness (Fig. 9); the laminates were prepared by vacuum filtration. The pressure-driven water flow, by vacuum suction, was inversely proportional to the thickness of the GO laminate. The water penetration flux J_x via a membrane can be expressed using the following relationship:

$$J_x = \Pi \frac{\Delta p}{\delta} \quad (3)$$

where Π is the permeability of the membrane, δ is the thickness of the membrane, and Δp is the equivalent pressure difference between the membrane according to the driving force (i.e., hydrostatic pressure or capillary action). The permeability in the trend line was $2.08 \times 10^{-5} \text{ m}^2/\text{bar h}$, close to the value of $1.83 \times 10^{-5} \text{ m}^2/\text{bar h}$ in the previous research [17].

Next, the nanocapillary speed U_x is discussed through consideration of the nanochannels in the GO laminate and its derivation from the water penetration flux. It was suggested that: (i) GO flakes have a characteristic length L of $1 \mu\text{m}$, as measured in the inset of Fig. 4(b), (ii) the effective area of the water flow channels is typically $L \times d$ for a flake unit area of L^2 [17], where d is the

interlayer distance between the GO flakes, (iii) the water molecules pass the nanochannel while keeping the molecular arrangement of the square lattice of the ice bilayer with AA stacking, as discussed above [34], and (iv) the effective channel length for the water molecules to travel to meet the base of the mushroom bubble is dependent on the depth x of the GO laminate film from its top surface, which directly affects the nanocapillary speed.

The inset in Fig. 9 provides a further explanation of assumption (iv). Inflowing water molecules via nanochannels far from the top surface (lower line) should penetrate over a longer effective channel length to reach the base of the mushroom bubble, compared with those near the top surface (upper line). That is, water molecules should penetrate the depth of the GO laminate film, resulting in a reduction in the penetration speed. This should be considered a representative penetration speed of water molecules in the lateral direction over the entire film thickness. This is the reason why the nanocapillary speed was derived with the subscript x .

Using the reasoning above, the nanocapillary speed of the water molecules via nanochannels between GO flakes was derived by a mass balance equation based on the number of water molecules escaping the channel. The water molecules were arranged into an effective channel with a bilayer thickness and width of L , as follows:

$$\frac{J_x L^2 \rho_l N_A}{M_w} = 2 \frac{L}{l_{\text{ice}}} \frac{U_x}{l_{\text{ice}}} \quad (4)$$

where M_w , ρ_l , and N_A are the molecular weight, liquid density, and Avogadro number, respectively. Moreover, l_{ice} is the intermolecular distance of ice with a square lattice, reported as 2.83 \AA [34]. The left side of Eq. (4) indicates the number rate of penetrating water molecules via a unit area of L^2 ; the right side indicates that of the equivalent flow channel in the GO laminate, as shown in Fig. 7(e): the first term is the bilayer, the second is the number of arranged water molecules along width L , and the third is the number rate of penetrating water molecules in the flow direction. Here, it is worth to mention that the nanocapillary speed U_x represented horizontal direction, even though water penetration flux J_x was measured in the cross-plane direction. The GO laminate consists of GO flakes having large aspect ratio, which means a wide sheet shape ($\sim 1 \mu\text{m}$) with very thin thickness ($\sim 1 \text{ nm}$), as shown in the inset of Fig. 4(b). Because of this, the equivalent channel length could be a thousand times of film thickness, in which water molecules should transfer the nanochannels layered in the horizontal direction with the surface in order to penetrate the GO laminate: $l_{\text{eff}} = L \delta_{\text{film}}/d$.

According to Eqs. (3) and (4), it is important to determine an equivalent nanocapillary pressure. MD simulations of nanocapillarity reported $\sim 1000 \text{ bar}$ of equivalent capillary pressure for van der Waals forces [17,18], but this cannot be applied to a macroscopic water flow [37]. In an evaporation process, as soon as the water molecule exited the channel, a neighboring water molecule would fill the vacancy to maintain water-saturation of the GO laminate. The evaporation on the GO laminate was supposed to be related with molecular diffusion of nanoconfined water molecules in GO nanochannels, rather than the directional motion by external work. Therefore, we postulated that the maximum speed of water molecules would be limited by its maximum diffusion speed in GO nanochannels.

Sun et al. [19] measured the water exchange rate via GO membrane ($4 \mu\text{m}$ thick) between two water reservoirs in no external force, i.e., same hydraulic head; it meant the diffusion rate of water in the water-saturated GO laminate. Deuterium oxide (D_2O) was employed as a tracer for isotope labeling with Fourier transform infrared (FTIR) spectroscopy. Initial volume fraction of D_2O in source reservoir was controlled up to 70%, the exchange rate was measured by its concentration in drain reservoir responded with time. Accordingly, diffusion-induced water penetration rate of water via GO membrane could be measured. They concluded

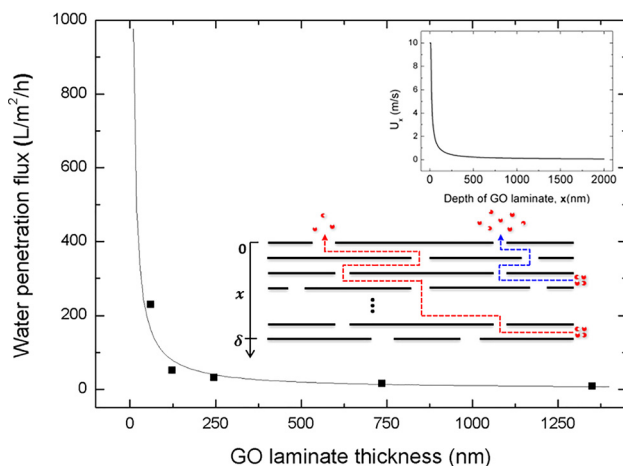


Fig. 9 Water penetration flux according to thickness of the GO laminate and evaluation of the nanocapillary speed of water molecules. (Inset graph) nanocapillary speed according to depth of the GO laminate. (Inset schematics) the water molecules should penetrate the longer (shorter) effective nanochannels to reach the boiling surface according to the depth of the GO laminate film, as indicated by the lower (upper) line, which causes as reduction in their speed.

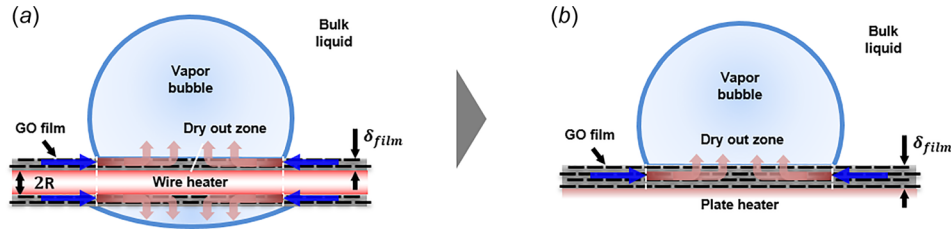


Fig. 10 Comparison of liquid inflow to evaluate the equivalent thickness of a GO laminate on wire heater geometry: (a) a wire heater and (b) a plate heater (arrow inside bubble: liquid evaporation, arrow outside bubble: liquid supply)

that the diffusion coefficient through efficient GO nanochannels were 4–5 orders of magnitude higher than that through cellulose filter with submicrometer-sized pore; the effective diffusivity of GO nanochannel D_{eff} was $1.52 \times 10^{-4} \text{ m}^2/\text{s}$. From 1D Fick's first law [38], the nanocapillary speed could be estimated as $U_x = D_{\text{eff}}/l_{\text{eff}} = D_{\text{eff}}d/L\delta_{\text{film}}$. Using Eqs. (3) and (4), the equivalent nanocapillary pressure was expected to be 11.3 bar.

Using the inverse proportional relationship between J_x and the thickness of the GO laminate δ_{film} , the measured permeability, and the equivalent nanocapillary pressure, the nanocapillary speed, U_x , according to the depth of GO film was plotted using Eqs. (3) and (4) (inset in Fig. 9). The nanocapillary speed showed a sharp increase as the depth of the GO laminate film decreased. In a previous study, water molecules confined in the nanochannel with a 1 nm effective channel height showed a bilayer arrangement and a penetration speed of 10 m/s under MD simulation [24]. In this study, the water penetration speed reached the same value predicted using MD simulation (10 m/s) when the depth of the GO laminate film was thinner than 10 nm. It was reasoned from MD simulations that the water penetration speed had a limit of 10 m/s to incorporate a singularity in Eq. (3).

Now, we could evaluate the effect of nanocapillarity on CHF enhancement, using Eq. (2). Because the water molecules form a bilayer in the interlayer space between the GO flakes in the laminate film [18,23,24], the number of water molecules along the film thickness of δ_{film} can be evaluated using $N = 2\delta_{\text{film}}/d$. The interlayer distance d of the GO flakes reportedly varies from 7 to 13 Å, according to the relative humidity [17,32,33]. SEM observations used to measure the thickness of the GO laminate were carried out at nearly zero humidity, corresponding to an interlayer distance d of 7 Å. To analyze the penetrating water bilayers for each individual GO interlayer channel in an effective continuum water inflow, the intermolecular distance of water in a liquid state was simplified to $\bar{l} = [M_w/(\rho_l N_A)]^{1/3}$. Thus, the porosity, ε , i.e., the effective ratio for inflowing water molecules to occupy the entire film thickness, can be expressed as follows:

$$\varepsilon = \frac{N\bar{l}}{\delta_{\text{film}}} = \frac{2}{d} \left(\frac{M_w}{\rho_l N_A} \right)^{1/3} \quad (5)$$

The departing bubble radius with a contact angle of 60 deg was estimated as 2.9 mm, by a force balance between its buoyancy and surface tension. With Eqs. (2) and (5), the attainable heat flux gain by water penetration for CHF enhancement was estimated from the heat balance between the latent heat of liquid inflow and transferred heat into the square area of the departing bubble diameter [1], as follows:

$$\begin{aligned} q''_{\text{gain_water penetration}} &= C \frac{h_{\text{lg}} \rho_l Q}{4r_b^2} \\ &= C \frac{\pi h_{\text{lg}} \rho_l}{r_b d} \left(\frac{M_w}{\rho_l N_A} \right)^{1/3} \sin \theta^* \int_0^{\delta_{\text{film}}} U_x dx \quad (6) \end{aligned}$$

A prediction of CHF enhancement from the water penetration analysis, using Eq. (6), is presented in Fig. 6. The expected CHF gain demonstrated well the trend of CHF enhancement data according to the thickness of the GO laminate with the same order of magnitude (correction factor C of 1.7).

In the previous research [12], we conducted similar experiments to evaluate CHF performance in GO colloidal suspensions with Nichrome wire heaters. Similarly, GO laminate structures were formed on the wire heater by deposition of GO flakes; marked CHF enhancement was observed.

To predict CHF enhancement of a GO laminate on a wire heater, it was necessary to adopt an effective thickness to consider the geometrical difference between a wire heater and a plate heater. It was supposed that a departing bubble on a wire heater was the same as that on a plate heater for simplicity, although the force interaction between surface tension and buoyancy force would be expected to change according to the heater geometry. The base area of a departing bubble for water inflow on a wire heater can be determined with the wire heater diameter, D , so that the effective thickness can be derived, as follows (Fig. 10):

$$4\pi R \delta_{\text{film}} = 2\pi r_b \sin \theta^* \delta_{\text{effective}} \quad (7)$$

$$\delta_{\text{effective}} = \frac{2R \delta_{\text{film}}}{r_b \sin \theta^*} \quad (8)$$

Figure 6 shows the CHF prediction for a GO laminate on a wire heater using the effective thickness as well as that for a plate heater, and the prediction by nanocapillarity using Eqs. (6) and (8). Equation (6) well predicted the rapid increase in the CHF value before the saturation region of CHF enhancement, which was predicted in CHF experiments using plate heaters. We thus conclude that the nanocapillarity analysis predicted the CHF characteristics of the GO laminate on a wire heater and a plate heater: rapid CHF enhancement followed by saturation.

4 Conclusion

We investigated the nanocapillary flow speed of water through the GO laminate film and its enhancement of the CHF under pool boiling when used as surface coating. We speculated that the laminate film enhances water transport and prevents the formation of dry regions (thus enhancing CHF by up to 140%). We estimate the nanocapillary flow using the measured water penetration rate through a GO laminate, which was measured with the controlled variable film thickness. The nanocapillary flow speed is inversely proportional to the effective channel length (film thickness) and reaches a maximum speed of 10 m/s with a permeability of $2.08 \times 10^{-5} \text{ m}^2/\text{bar h}$ and an equivalent nanocapillary pressure of 11.2 bar. With the CHF enhancement and its plateau with an increase in the GO laminate thickness, we anticipate its application in boiling heat transfer and beyond.

Acknowledgment

This research was supported by the Incheon National University (International Cooperative) Research Grant in 2014.

Nomenclature

c_{colloids}	= concentration of GO colloids (g/m^3)
d	= interlayer distance between GO flakes (m)
D_{eff}	= effective diffusivity of GO nanochannel (m^2/s)
h_{lg}	= latent heat of water (kJ/kg)
J_x	= water penetration flux ($\text{m}^3/\text{m}^2 \text{ s}$)
K	= correction factor
L	= width of GO flake (m)
\bar{l}	= intermolecular distance of water in a liquid state (m)
\bar{l}_{ice}	= intermolecular distance of ice with a square lattice (m)
M_w	= molecular weight (kg/mol)
N	= number of water molecules along the film thickness (#)
N_A	= Avogadro number ($\#/\text{mol}$)
Q	= water penetration rate (m^3/s)
$q''_{\text{gain_water penetration}}$	= attainable heat flux gain (kW/m^2)
R	= diameter of wire heater (m)
r_b	= departing bubble radius (m)
U_x	= nanocapillary speed (m/s)
V_{colloids}	= volume of the GO colloids (m^3)
Δp	= equivalent pressure difference (Pa)
δ	= thickness of the membrane (m)
δ_{film}	= thickness of GO film (m)
$\delta_{\text{effective}}$	= effective thickness of GO film (m)
ε	= porosity
θ^*	= receding contact angle (deg)
Π	= permeability of the membrane ($\text{m}^2/\text{s Pa}$)
ρ_{GO}	= density of GO film (kg/m^3)
ρ_l	= density of liquid water (kg/m^3)

References

- [1] Kim, H. D., and Kim, M. H., 2007, "Effect of Nanoparticle Deposition on Capillary Wicking That Influences the Critical Heat Flux in Nanofluids," *Appl. Phys. Lett.*, **91**(1), p. 014104.
- [2] Rahman, M. M., Ölçeroğlu, E., and McCarthy, M., 2014, "Role of Wickability on the Critical Heat Flux of Structured Superhydrophilic Surfaces," *Langmuir*, **30**(37), pp. 11225–11234.
- [3] Chu, K.-H., Enright, R., and Wang, E. N., 2012, "Structured Surfaces for Enhanced Pool Boiling Heat Transfer," *Appl. Phys. Lett.*, **100**(24), p. 241603.
- [4] Chu, K.-H., Soo Joung, Y., Enright, R., Buie, C. R., and Wang, E. N., 2013, "Hierarchically Structured Surfaces for Boiling Critical Heat Flux Enhancement," *Appl. Phys. Lett.*, **102**(15), p. 151602.
- [5] Ahn, H. S., Jo, H. J., Kang, S. H., and Kim, M. H., 2011, "Effect of Liquid Spreading Due to Nano/Microstructures on the Critical Heat Flux During Pool Boiling," *Appl. Phys. Lett.*, **98**(7), p. 071908.
- [6] Ahn, H. S., Park, G., Kim, J., and Kim, M. H., 2012, "Wicking and Spreading of Water Droplets on Nanotubes," *Langmuir*, **28**(5), pp. 2614–2619.
- [7] Zuber, N., 1959, "Hydrodynamic Aspects of Boiling Heat Transfer," *Ph.D. thesis*, University of California, Los Angeles, Los Angeles, CA.
- [8] Park, S. D., Won Lee, S., Kang, S., Bang, I. C., Kim, J. H., Shin, H. S., Lee, D. W., and Won Lee, D., 2010, "Effects of Nanofluids Containing Graphene/Graphene-Oxide Nanosheets on Critical Heat Flux," *Appl. Phys. Lett.*, **97**(2), p. 023103.
- [9] Ahn, H. S., Kim, J. M., and Kim, M. H., 2013, "Experimental Study of the Effect of a Reduced Graphene Oxide Coating on Critical Heat Flux Enhancement," *Int. J. Heat Mass Transfer*, **60**, pp. 763–771.
- [10] Ahn, H. S., Kim, J. M., Park, C., Jang, J. W., Lee, J. S., Kim, H., Kaviany, M., and Kim, M. H., 2013, "A Novel Role of Three Dimensional Graphene Foam to Prevent Heater Failure During Boiling," *Sci. Rep.*, **3**, p. 01960.
- [11] Ahn, H. S., Kim, J. M., Kim, T., Park, S. C., Kim, J. M., Park, Y., Yu, D. I., Hwang, K. W., Jo, H., Park, H. S., Kim, H., and Kim, M. H., 2014, "Enhanced Heat Transfer is Dependent on Thickness of Graphene Films: The Heat Dissipation During Boiling," *Sci. Rep.*, **4**, p. 6276.
- [12] Kim, J. M., Kim, T., Kim, J., Kim, M. H., and Ahn, H. S., 2014, "Effect of a Graphene Oxide Coating Layer on Critical Heat Flux Enhancement Under Pool Boiling," *Int. J. Heat Mass Transfer*, **77**, pp. 919–927.
- [13] Kim, J. M., Kim, J. H., Park, S. C., Kim, M. H., and Ahn, H. S., 2016, "Nucleate Boiling in Graphene Oxide Colloids: Morphological Change and Critical Heat Flux Enhancement," *Int. J. Multiphase Flow*, **85**, pp. 209–222.
- [14] Arik, M., and Bar-Cohen, A., 2003, "Effusivity-Based Correlation of Surface Property Effects in Pool Boiling CHF of Dielectric Liquids," *Int. J. Heat Mass Transfer*, **46**(20), pp. 3755–3764.
- [15] Kandlikar, S. G., 2001, "A Theoretical Model to Predict Pool Boiling CHF Incorporating Effects of Contact Angle and Orientation," *ASME J. Heat Transfer*, **123**(6), pp. 1071–1079.
- [16] Liter, S. G., and Kaviany, M., 2001, "Pool-Boiling CHF Enhancement by Modulated Porous-Layer Coating: Theory and Experiment," *Int. J. Heat Mass Transfer*, **44**(22), pp. 4287–4311.
- [17] Nair, R. R., Wu, H. A., Jayaram, P. N., Grigorieva, I. V., and Geim, A. K., 2012, "Unimpeded Permeation of Water Through Helium-Leak-Tight Graphene-Based Membranes," *Science*, **335**(6067), pp. 442–444.
- [18] Joshi, R. K., Carbone, P., Wang, F. C., Kravets, V. G., Su, Y., Grigorieva, I. V., Wu, H. A., Geim, A. K., and Nair, R. R., 2014, "Precise and Ultrafast Molecular Sieving Through Graphene Oxide Membranes," *Science*, **343**(6172), pp. 752–754.
- [19] Sun, P., Liu, H., Wang, K., Zhong, M., Wu, D., and Zhu, H., 2015, "Ultrafast Liquid Water Transport Through Graphene-Based Nanochannels Measured by Isotope Labelling," *Chem. Commun.*, **51**(15), pp. 3251–3254.
- [20] Tong, W. L., Ong, W.-J., Chai, S.-P., Tan, M. K., and Hung, Y. M., 2015, "Enhanced Evaporation Strength Through Fast Water Permeation in Graphene-Oxide Deposition," *Sci. Rep.*, **5**, p. 11896.
- [21] Caupin, F., Cole, M. W., Balibar, S., and Treiner, J., 2008, "Absolute Limit for the Capillary Rise of a Fluid," *Europhys. Lett.*, **82**(5), p. 56004.
- [22] Qiao, Y., Xu, X., and Li, H., 2013, "Conduction of Water Molecules Through Graphene Bilayer," *Appl. Phys. Lett.*, **103**(23), p. 233106.
- [23] Boukhalval, D. W., Katsnelson, M. I., and Son, Y.-W., 2013, "Origin of Anomalous Water Permeation Through Graphene Oxide Membrane," *Nano Lett.*, **13**(8), pp. 3930–3935.
- [24] Wei, N., Peng, X., and Xu, Z., 2014, "Breakdown of Fast Water Transport in Graphene Oxides," *Phys. Rev. E: Stat. Nonlinear Soft Matter Phys.*, **89**(1), p. 012113.
- [25] Koenig, S. P., Wang, L., Pellegrino, J., and Bunch, J. S., 2012, "Selective Molecular Sieving Through Porous Graphene," *Nat. Nanotechnol.*, **7**(11), pp. 728–732.
- [26] Huang, H., Song, Z., Wei, N., Shi, L., Mao, Y., Ying, Y., Sun, L., Xu, Z., and Peng, X., 2013, "Ultrafast Viscous Water Flow Through Nanostrand-Channelled Graphene Oxide Membranes," *Nat. Commun.*, **4**, p. 2979.
- [27] Paul, D. R., 2012, "Creating New Types of Carbon-Based Membranes," *Science*, **335**(6067), pp. 413–414.
- [28] Li, D., Muller, M. B., Gilje, S., Kaner, R. B., and Wallace, G. G., 2008, "Processable Aqueous Dispersions of Graphene Nanosheets," *Nat. Nanotechnol.*, **3**(2), pp. 101–105.
- [29] Dikin, D. A., Stankovich, S., Zimney, E. J., Piner, R. D., Dommett, G. H. B., Evmenenko, G., Nguyen, S. T., and Ruoff, R. S., 2007, "Preparation and Characterization of Graphene Oxide Paper," *Nature*, **448**(7152), pp. 457–460.
- [30] Cote, L. J., Kim, F., and Huang, J., 2008, "Langmuir–Blodgett Assembly of Graphite Oxide Single Layers," *J. Am. Chem. Soc.*, **131**(3), pp. 1043–1049.
- [31] Haramura, Y., and Katto, Y., 1983, "A New Hydrodynamic Model of Critical Heat Flux, Applicable Widely to Both Pool and Forced Convection Boiling on Submerged Bodies in Saturated Liquids," *Int. J. Heat Mass Transfer*, **26**(3), pp. 389–399.
- [32] Lerf, A., Buchsteiner, A., Pieper, J., Schöttl, S., Dekany, I., Szabo, T., and Boehm, H. P., 2006, "Hydration Behavior and Dynamics of Water Molecules in Graphite Oxide," *J. Phys. Chem. Solids*, **67**(5–6), pp. 1106–1110.
- [33] Cerveny, S., Barroso-Bujans, F., Alegria, A., and Colmenero, J., 2010, "Dynamics of Water Intercalated in Graphite Oxide," *J. Phys. Chem. C*, **114**(6), pp. 2604–2612.
- [34] Algara-Siller, G., Lehtinen, O., Wang, F. C., Nair, R. R., Kaiser, U., Wu, H. A., Geim, A. K., and Grigorieva, I. V., 2015, "Square Ice in Graphene Nanocapillaries," *Nature*, **519**(7544), pp. 443–445.
- [35] Andrikopoulos, K. S., Bounos, G., Tasis, D., Sygellou, L., Drakopoulos, V., and Voyiatzis, G. A., 2014, "The Effect of Thermal Reduction on the Water Vapor Permeation in Graphene Oxide Membranes," *Adv. Mater. Interfaces*, **1**(8), p. 2400250.
- [36] Duan, C., Karnik, R., Lu, M.-C., and Majumdar, A., 2012, "Evaporation-Induced Cavitation in Nanofluidic Channels," *Proc. Natl. Acad. Sci.*, **109**(10), pp. 3688–3693.
- [37] Kaviany, M., 2012, *Principles of Heat Transfer in Porous Media*, Springer Science & Business Media, New York.
- [38] Bird, R. B., Stewart, W. E., and Lightfoot, E. N., 1960, *Transport Phenomena*, Wiley, New York, p. 413.